6.0 PHYSICAL OCEANOGRAPHIC CHARACTERIZATION

Recommended Citation:

O'Donnell, J., McCardell, G., Howard-Strobel, M.M. (2021). "Physical Oceanographic Characterization" p. 239-261 in "The Long Island Sound Habitat Mapping Initiative Phase II – Eastern Long Island Sound – Final Report" (Unpublished project report).

6.1 New Data Acquisition

We executed springtime and wintertime deployments of bottom tripods with an array of instruments measuring temperature, salinity, currents, and stresses and executed two ship surveys in which we measured salinity, temperature, density structure and current patterns.

Tripod-style bottom-frames were deployed in and near Fishers Island Sound to collect measurements for determining bottom stresses, current structure, wave characteristics, salinity, and temperature. Three frames were deployed in spring 2017 and five during winter 2018. Tables 6.1-1 and 6.1-2 summarize the frame deployments for fall 2017 and winter 2018, respectively; Figs. 6.1-1 and 6.1-2 show the frame deployment locations for fall 2017 and winter 2018, respectively. These observations supplement previous data from eastern Long Island Sound.

The moored instrument array configuration for the frames is shown in Figure 6.1-3. Each frame was equipped with an RDI acoustic Doppler current profiler (ADCP) with wave sampling enabled located 1.5 meters above bottom, a Nortek Aquadopp 2 kHz High-Resolution phase coherent profiler looking downward at 0.75 meters above the bottom, and a Sea-Bird Model 37 SMP measuring salinity, temperature and pressure also at 0.75 meters above bottom. The RDI ADCP sampled currents every 15 minutes and waves once per hour. The Nortek Aquadopp sampled every hour, and the Sea-Bird CT/P sensor sampled every 15 minutes.

Transect and station data were collected during fall 2017 and spring 2018 cruises. During both cruises, a single transect was continually and repeatedly sampled during a 12-hour period with a ship-mounted acoustic Doppler current profiler (ADCP). Stations along the transect were also repeatedly sampled with a Sea-Bird Model 19+ CTD (conductivity, temperature, depth). During the fall 2017 cruise, four stations were sampled. During the spring 2018 cruise, additional stations were added to look at cross-bathymetric contours in the eastern half and the eastern entrance to Fishers Island Sound, and near the western limit of the study area south of Clinton Harbor. Cruise data collection summaries are presented in Tables 6.1-3 and 6.1-4. Location details of the cruise sampling stations are shown in the appendix. Table 6.1-5 shows the timeline of the data collection effort.

Table 6.1- 1. Spring 2017 Moored Frames - Station Location and Deployment Summary.

Station ID	Latitude	Longitude	Sensors	Deploy Date (2017)	Recovery Date (2017)	Water Depth (m)	Deployment Length (days)
SOW1	41.303300°	-71.903817°	-AQD 2 kHz HR -SBE37 CT/P -ADCP 600 kHZ	30 MAR	7 JUN	22.6	70
EID2	41.325933°	-71.927667°	-AQD 2 kHz HR -SBE37 CT/P -ADCP 1200 kHz	28 MAR	7 JUN	4.6	72
WID3	41.310900°	-71.968917°	-AQD 2 kHz HR -SBE37 CT/P -ADCP 1200 kHz	28 MAR	8 JUN	5.5	73

Table 6.1- 2. Winter 2017-2018 Moored Frames - Station Location and Deployment Summary.

Station ID	Latitude	Longitude	Station Depth (meters)	RDI ADCP SN/Freq	SBE 37 SN	AQD SN
SOW1	41 18.1977	-71 54.2284	21.5	1094/600	9695	8445
EID2	41 19.5557	-71 55.6593	3.9	10463/1200	9673	8455
WID3	41 18.6537	-71 58.1355	4.8	10462/1200	9696	8432
WFW4	41 17.4727	-72 02.2383	10.3	6615/600	9694	8438
SFW5	41 16.2218	-71 58.3172	6.3	11708/1200	9674	8554

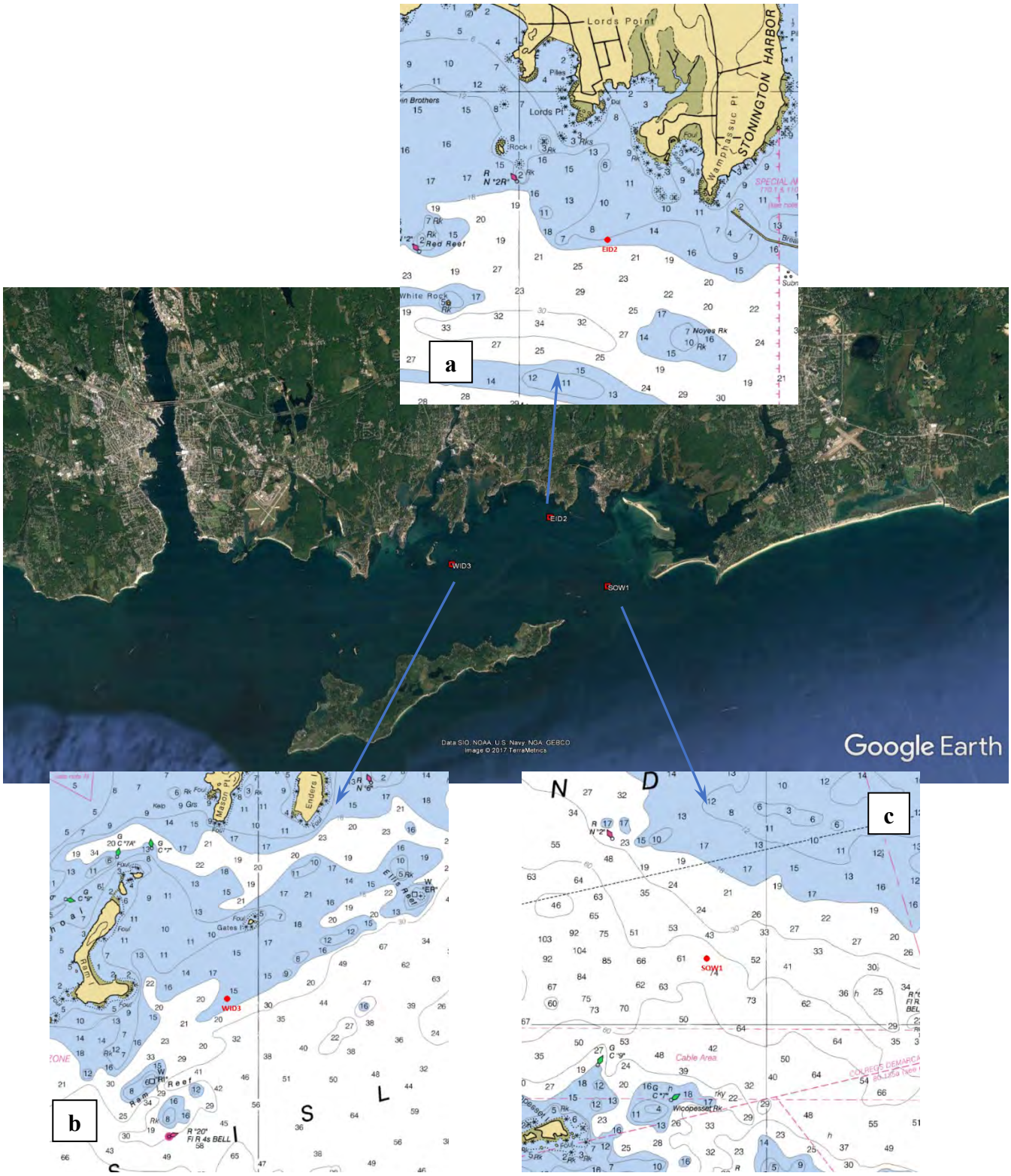

Figure 6.1- 1 Location of the three frames deployed in Fishers Island Sound during Spring of 2017, a) detail of bathymetry (in feet) near EID2 - the Eastern Inside Dissipative station, b) bathymetry (in feet) at WID3 - Western Inside Dissipative station, c) bathymetry (in feet) at SOW1 - Southern Outside Wave station.

Figure 6.1- 2. Location of the five bottom moored frames in Fishers Island Sound for the Winter 2017-2018 data collection campaign. Yellow stations were occupied during the Spring 2017 campaign, the two red stations are new locations.

Figure 6.1- 3 Frame deployed at SOW1 – all frames were equipped similarly, with a) Nortek High Resolution downward looking Aquadopp profiler, b) Sea-Bird Instruments Model 37 SMP Conductivity/Temperature/Pressure sensor, and c) RD Instruments acoustic Doppler current profiler with wave array firmware.

Table 6.1- 3. CTD 12 Hour Survey – Winter 2017 - Station Locations.

Station ID	Latitude	Longitude	Station Depth (meters)	N Casts
N1-1	41 17.9177	72 05.0212	6.1	5
N1-2	41 17.1696	72 05.4720	10.9	10
N1-3	41 16.4313	72 05.9873	20.1	10
N1-4	41 15.5349	72 06.5856	33.5	6
N2-1	41 18.1732	72 10.7515	9.8	6
N2-2	41 17.3729	72 10.7154	14.0	12
N2-3	41 16.5301	72 10.6272	17.7	12
N2-4	41 15.5604	72 10.5426	32.6	7
N3-1	41 17.1089	72 14.6969	16.5	6
N3-2	14 16.1559	72 14.6969	17.4	11
N3-3	41 15.2662	72 14.6969	28.0	11
N3-4	41 14.3049	72 14.6969	33.8	6
N4-1	41 15.5647	72 20.4353	5.8	6
N4-2	41 15.0995	72 19.6817	8.5	11
N4-3	41 14.5568	72 18.7853	32.3	11
N4-4	41 13.9125	72 17.7541	36.6	6
N5-1	41 17.7994	72 02.5349	9.1	8
N5-2	41 16.8567	72 02.5349	12.5	8
N5-3	41 17.3042	72 00.0604	14.0	8
N5-4	41 18.1633	72 00.0604	9.8	9

Table 6.1- 4. CTD 12 Hour Survey - Spring 2018 - Station Locations.

Station ID	Latitude	Longitude	Station Depth (meters)	N Casts
N0-1	41 17.6108	71 51.4745	21.1	7
N0-2	41 17.0093	71 53.4086	22.0	7
N0-3	41 16.3598	71 53.0402	42.9	7
N0-4	41 17.0412	71 51.0424	36.7	8
N1-1	41 18.8733	71 55.3366	9.5	8
N1-2	41 18.8733	71 57.3814	16.4	8
N1-3	41 18.0035	71 57.3814	19.4	8
N1-4	41 18.0035	71 55.3366	20.0	8
N21-1	41 17.9177	72 05.0212	6.1	7
N21-2	41 17.1696	72 05.4720	10.9	12
N21-3	41 16.4313	72 05.9873	20.1	13
N21-4	41 15.5349	72 06.5856	33.5	7
N22-1	41 18.1732	72 10.7515	9.8	6
N22-2	41 17.3729	72 10.7154	14.0	11
N22-3	41 16.5301	72 10.6272	17.7	12
N22-4	41 15.5604	72 10.5426	32.6	6
N23-1	41 17.1089	72 14.6969	16.5	6
N23-2	14 16.1559	72 14.6969	17.4	12
N23-3	41 15.2662	72 14.6969	28.0	12
N23-4	41 14.3049	72 14.6969	33.8	7
N24-1	41 15.5647	72 20.4353	5.8	6
N24-2	41 15.0995	72 19.6817	8.5	12
N24-3	41 14.5568	72 18.7853	32.3	12
N24-4	41 13.9125	72 17.7541	36.6	7
N6-1	41 14.7994	72 31.4255	9.8	7
N6-2	41 13.8567	72 31.4255	26.1	13
N6-3	41 13.3042	72 31.4255	32.5	13
N6-4	41 12.1633	72 31.4255	17.2	7

Table 6.1- 5. Data Collection Timeline.

2017	
28 March	Deploy WID3, EID2 in Fishers Island Sound
30 March	Deploy SOW1 east entrance FIS
07 June	Recover SOW1, EID2
08 June	Recover WID3
28 Nov-3 Dec	SeaBoss cruise -> underway ADCP
28-29 Nov	12 hour CTD survey stations N1-1, N1-2, N1-3, N1-4
29-30 Nov	12 hour CTD survey stations N2-1, N2-2, N2-3, N2-4
30 Nov-1 Dec	12 hour CTD survey stations N3-1, N3-2, N3-3, N3-4
01-02 Dec	12 hour CTD survey stations N4-1, N4-2, N4-3, N4-4
02-03 Dec	12 hour CTD survey stations N5-1, N5-2, N5-3, N5-4
21 Dec	Deploy WID3, EID2, SOW1, SFW5, WFW4
2018	
19 March	Recover WID3, EID2, SOW1, SFW5, WFW4
08-15 May	SeaBoss cruise -> underway ADCP and mTSG
08-09 May	12 hour CTD survey stations N1-1, N1-2, N1-3, N1-4
09-10 May	12 hour CTD survey stations N21-1, N21-2, N21-3, N21-4
10-11 May	12 hour CTD survey stations N22-1, N22-2, N22-3, N22-4
11-12 May	12 hour CTD survey stations N23-1, N23-2, N23-3, N23-4
12-13 May	12 hour CTD survey stations N24-1, N24-2, N24-3, N24-4
13-14 May	12 hour CTD survey stations N6-1, N6-2, N6-3, N6-4
14-15 May	12 hour CTD survey stations N0-1, N0-2, N0-3, N0-4

6.2 Model Implementation

The Long Island Sound (LIS) FVCOM model was initially developed with support from the Connecticut Sea Grant College Program and the collaboration of Professor C. Chen of the University of Massachusetts, Dartmouth. The domain of the model and the resolution are shown in Figure 6.2-1. We developed an implementation of FVCOM (Chen et al., 2007) at UCONN and designed it to use the results of the operational northwest Atlantic regional model, operated as the Northeast Coastal Forecast System (NECOFS) to provide ocean boundary conditions. This 'nesting' approach is computationally efficient since it allows the effect of the larger-scale processes to be simulated at coarse resolution through NECOFS and allows UCONN computing resources to focus on the smaller-scale structures in LIS and Block Island Sound (BIS). Our FVCOM implementation uses GOTM (Burchard, et al., 1999) to model vertical turbulent mixing. O'Donnell et al. (2015b) found that a bottom roughness value of z_0=1 cm provided the best representation of bed stresses within LIS in the FVCOM model and this value was used throughout the domain.

LIS-FVCOM was initialized using a temperature and salinity climatology data set derived via objective interpolation of CTDEEP station data as described by O'Donnell et al. (2015b), and the data in the NOAA archive described by Codiga and Ullman (2011). In order to be input

into the FVCOM model, these OI fields were linearly interpolated to a set of standard depths. The 2018 model runs were initialized using end-of-year conditions from 2017.

LIS-FVCOM is forced at the seaward boundaries by sea level variations and salinity and temperature. The sea level is initially prescribed using tidal constituents derived from the global tidal model (Egbert et al., 1994). The amplitudes and phases of the major constituents were then iteratively adjusted to achieve an optimal representation of the amplitude and phase at each tidal frequency using NOAA tidal height observations at Montauk (NY), New London (CT), New Haven (CT), Bridgeport (CT), and King's Point (NY). Subtidal fluctuations at the open boundary are incorporated from the NECOFS system by de-tiding and low-pass filtering the NECOFS solution at the open boundary locations using t-tide (Pawlowicz et al., 2002) and a 25-hour raised cosine low-pass filter. The model's subtidal performance was further optimized by removing the low-passed error in the NECOFS subtidal forcing as determined by comparing the NECOFS solution with NOAA sea-surface height (SSH) gauges at Newport, RI and Atlantic City, NJ. These stations are near the open boundary of the LIS model. The de-tided and adjusted NECOFS subtidal solution was then combined with the time series of tidal heights generated using the optimized tidal constituents as described above.

Freshwater enters the LIS FVCOM domain through seven model cells corresponding to the locations of the Thames, Connecticut, Niantic, Quinnipiac, Housatonic, and Hudson rivers and New York City wastewater treatment plants (WWTP). These fluxes are based on gauged flows measured by the USGS at Thompsonville, CT, and lagged by one day to account for the distance between the head of the Connecticut River in our model and Thompsonville. Each river, R_i, is adjusted using the USGS Thompsonville data as $R_i = 1.20 \frac{R_{CT}}{\overline{R_{CT}}} \overline{R_i}$ where R_{CT} is the day-specific Connecticut River flow, $\overline{R_{CT}}$ is the mean Connecticut River flow, and $\overline{R_i}$ is the mean flow for river *i*. The factor of 1.20 follows from the salt budget of Gay et al. (2004) and accounts for the portion of the watersheds of the rivers below the USGS gauges. A fixed input of 40 m^3s^{-1} was added to the East River to represent the freshwater discharged from the New York WWTPs.

Domain-variable winds derived from the Weather Research and Forecasting model (WRF) run as hindcasts at UMass, Dartmouth are used for the LIS-FVCOM surface wind forcing. The LIS-FVCOM model originally used heat fluxes also obtained from the UMass WRF model. However, the UMass WRF heat fluxes substantially underestimate the wintertime cooling at LIS locations. To correct this issue, we assimilated sea surface temperatures (SSTs) into the model using NASA MODIS Aqua 8-day composited and de-clouded (level 3) satellite data. Because the NASA SST product has poor coverage in cells that are close to the coast, we pre-screened the entire dataset to keep only data from cells that had at least 86.7% coverage for the entire year (i.e. we removed all data from those cells with 7 or more missing 8-day SSTs out of the total of 45 8-day products for the 2017 year). The remaining SST data was then linearly interpolated in time to fill any temporal gaps and then spatially interpolated to 100% coverage using the nearest spatial neighbor with good coverage. The net effect of this pre-screening and interpolation methodology is that values in cells at the coast where coverage is poor are replaced with the values from the nearest offshore cell.

Figure 6.2-1 shows time-series of the model to data temperature comparisons both with and without SST temperature assimilation. Note that the improvement in the bottom temperatures (panels a, b) is similar to the improvement in the surface temperatures (panel

c,d), indicating that the model is capturing the downward heat fluxes within the water column adequately.

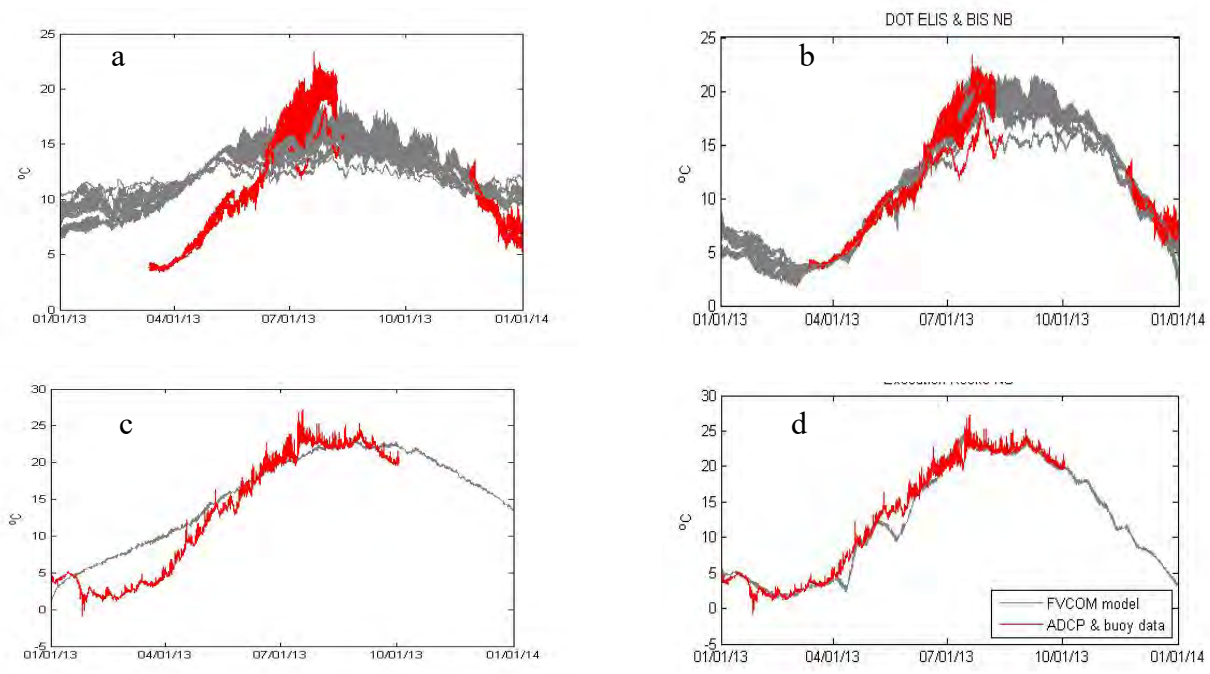

Figure 6.2- 1 Comparison of model temperature predictions (gray) with observations (red) in LIS during 2013 with and without SST data assimilation. (a,c) show comparisons when the model is forced using only WRF heat fluxes; (b,d) show the comparisons when MODIS-a SST is also assimilated into the model. (a,b) show comparisons of near-bottom temperatures at seven locations in the ELIS and BIS during 2013 (See O'Donnell et al., 2015a); (c,d) show comparisons of near-surface temperatures at the LISICOS Execution Rocks buoy.

6.3 Model Skill Assessment

To evaluate the model performance we use the 'skill', s, statistic defined as:

$$s = 1 - \frac{\left\langle \left(f_m - f_d \right)^2 \right\rangle}{\left\langle \left(f_d - \left\langle f_d \right\rangle \right)^2 \right\rangle} \qquad (1)$$

where f_m and f_d represent the model and data values (e.g. f represents sea level (η) or temperature (T), etc.) and the $\langle\ \rangle$ notation represents the mean of the argument over the simulation interval (i.e. $\langle f_d \rangle$ is the mean of the data) (von Storch and Zwiers, 1999).
The Long Island Sound model skill assessment using this metric is described in O'Donnell et al (2015). Since the time of that report, the model has been improved by Dr. McCardell. Most notably, the model now assimilates sea surface temperatures (SST) from the NASA MODIS Aqua satellite.

6.3.1 Sea Surface Height Skills

Table 6.3-1 shows the model sea-surface-height (SSH) skill (Equation 1) from the 2017 simulation compared to hourly measurements at the four NOAA tidal gauges in LIS: New London, New Haven, Bridgeport, and King's Point. The first row shows the skills when simulated sea surface heights (relative to MSL) are compared to the raw observations. The second and third rows shows the skills when the model and data series are divided into tidal and weather components using harmonic analysis (Pakolwicz et al, 2002). The errors in the simulation of tides are small - the skills all exceed 93%. The errors in the simulation of the total water level (SSH) mainly arise from the errors in the simulation of the meteorologically driven motions and are to some extent due to inadequacies in the atmospheric model used to prescribe winds.

Table 6.3- 1 Table 6.3.1: Model skills (Eq. 1) when model elevations are compared to NOAA gage data at New London, New Haven, Bridgeport, and Kings Point. The first row (Total SSH skill), shows the skills when sea-surface heights (relative to MSL) are compared, the the second row shows the skills at tidal frequencies, the third row shows the skills for the subtidal residuals.

	New London	New Haven	Bridgeport	King's Point
Total SSH skill	91%	92%	93%	93%
Tidal skill	94%	93%	94%	94%
Subtidal skill	77%	75%	77%	54%

Figure 6.3-1 shows a comparison of the spectral power density obtained from the NOAA record at the four LIS gauges with that from the LIS-FVCOM model at these locations. Note that although the model does a good job at capturing the M2 amplitudes and M4 harmonics, it significantly underestimates the M6 harmonics.

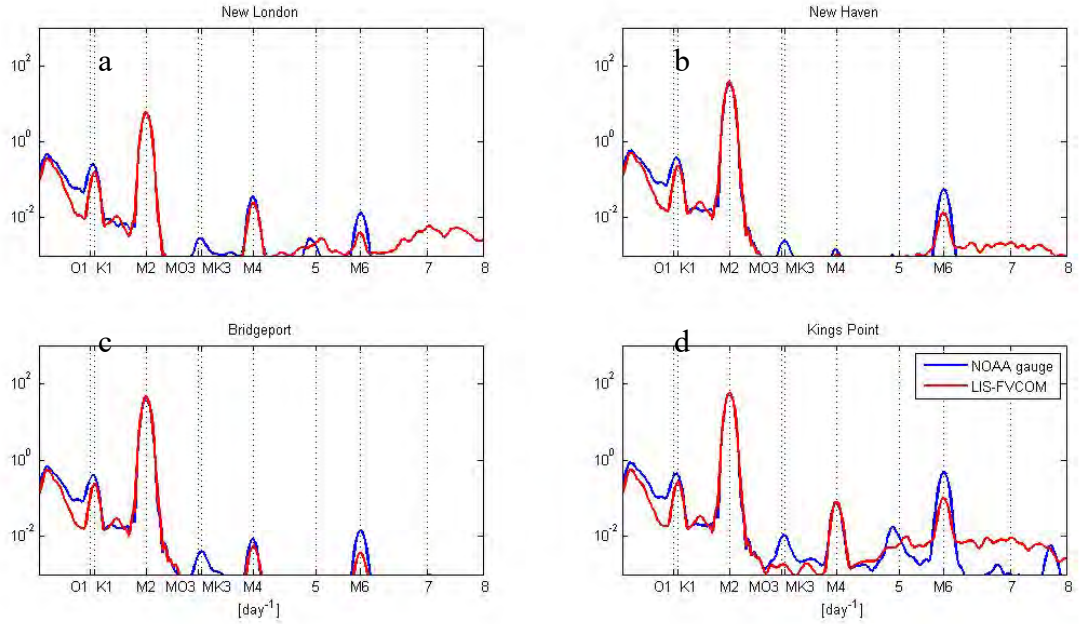

Figure 6.3- 1 Comparison of the power spectral density (PSD) of the SSH records from the NOAA gauges (blue) at New London (a), New Haven (b), Bridgeport (c), and Kings Point (d) with those from the FVCOM-LIS model (red) estimated using the Welch method with non-overlapping 10-day windows.

6.3.2 Temperature and Salinity Skills

Figure 6.3-2 shows a comparison of surface and bottom model temperatures with monthly climatologies derived from 1993-2015 CTDEEP surveys and the 2017 CTDEEP surveys. These data are described by Kaputa and Olson (2000) and O'Donnell et al. (2014). The skills listed in the panels were calculated by combining the individual station scores using the mean square methodology described in Ganju et al. (2016).

For comparison, the surface and bottom traditional skills from runs that only used the WRF heat flux forcing (did not use the SST assimilation) were in the 0.70-0.90 range. Note that the CTDEEP dataset used to evaluate the temperature skills shown in Figure 6.3.2 was not what was assimilated into the model. The high skill scores are thus indicative of both the success of the data assimilation itself and of excellent agreement between the screened remote sensing temperature data and the in situ temperature measurements made by the CTDEEP.

As shown in Figure 6.3-3, the near-surface and near-bottom traditional salinity skills are 0.15, and 0.19, respectively. Figure 6.3-3 indicates that much of the salinity error is due to a bias error. This was removed prior to creating the interpolated map products.

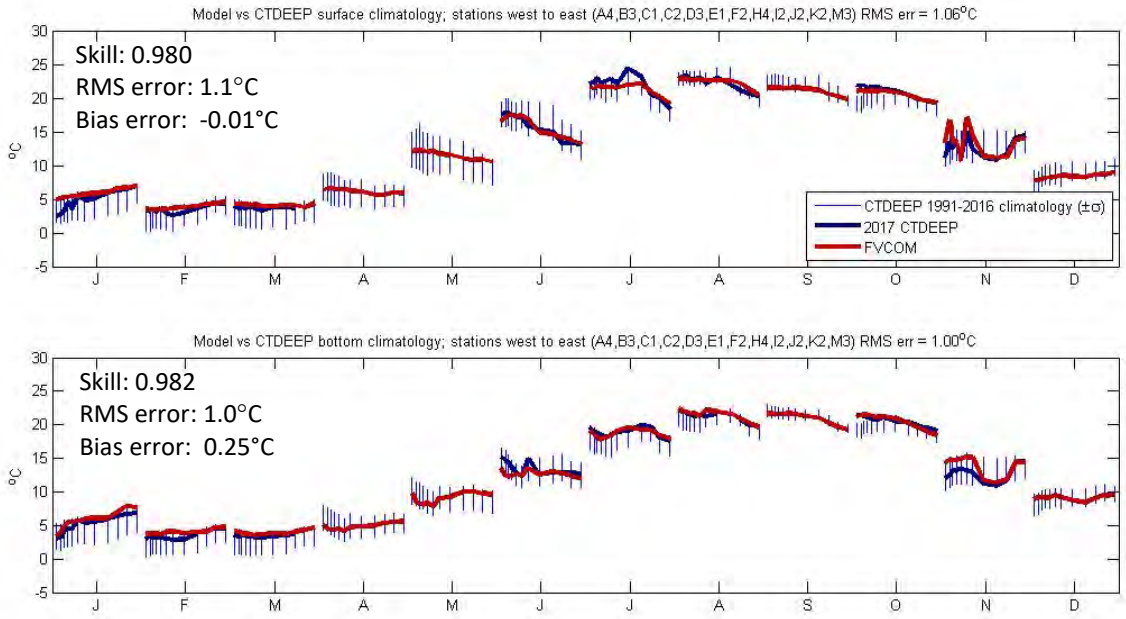

Figure 6.3- 2. Plots by month showing surface (top panel) and bottom (bottom panel) temperature comparisons between model predictions (red lines) and monthly climatologies from 1993-2016 CTDEEP survey data (thin vertical blue bars, ±σ) and the 2017 CTDEEP surveys (thick blue lines). Within each month, the CTDEEP stations are plotted by longitude from west to east.

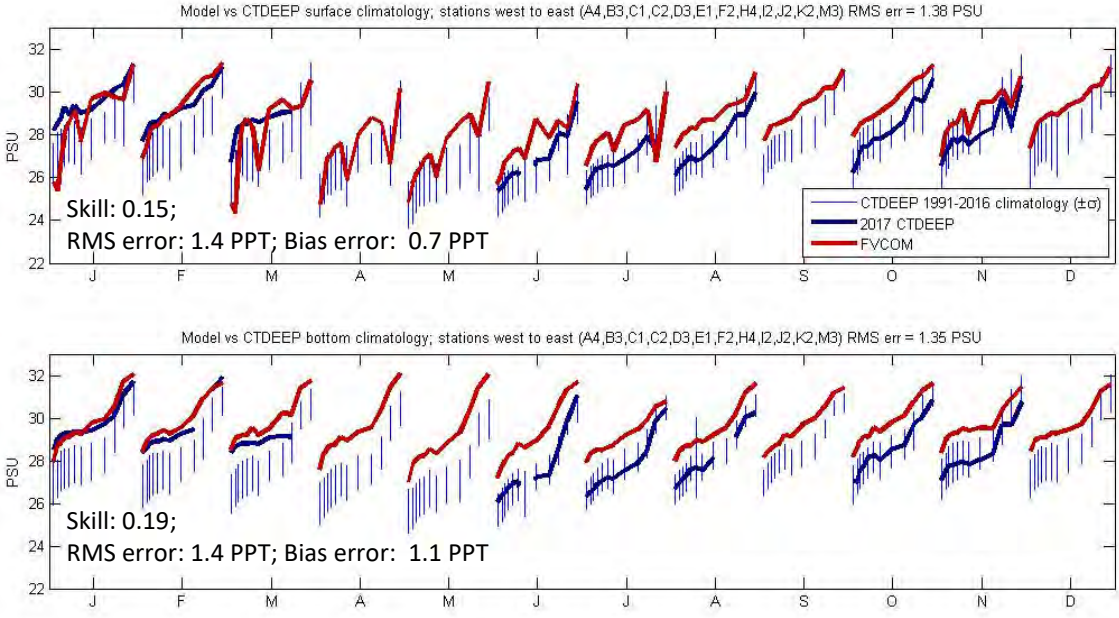

Figure 6.3- 3 Figure 6.3-3. Plots by month showing surface (top panel) and bottom (bottom panel) salinity comparisons between model predictions (red lines) and monthly climatologies from 1993-2016 CTDEEP survey data (thin vertical blue bars, ±σ) and the 2017 CTDEEP surveys (thick blue lines). Within each month, the CTDEEP stations are plotted by longitude from west to east.

6.4 Fisher's Island Sound (FIS) comparisons

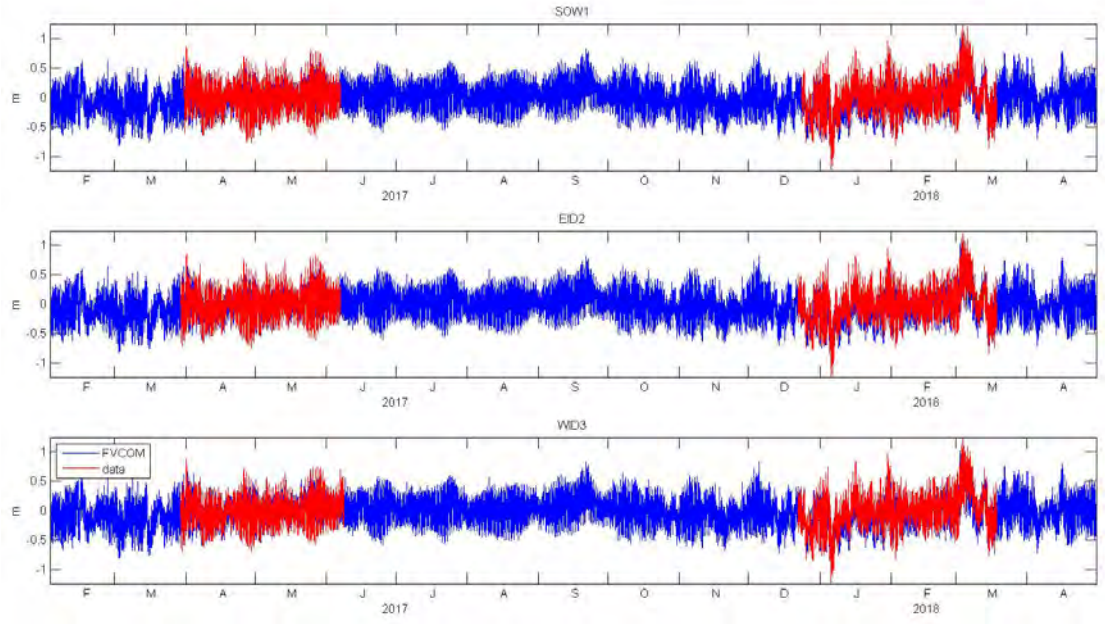

Figure 6.4- 1. Time-series plots of SSH at the three FIS bottom-mooring deployment locations comparing the FVCOM predictions (blue) with measurements from the moored instruments (red).

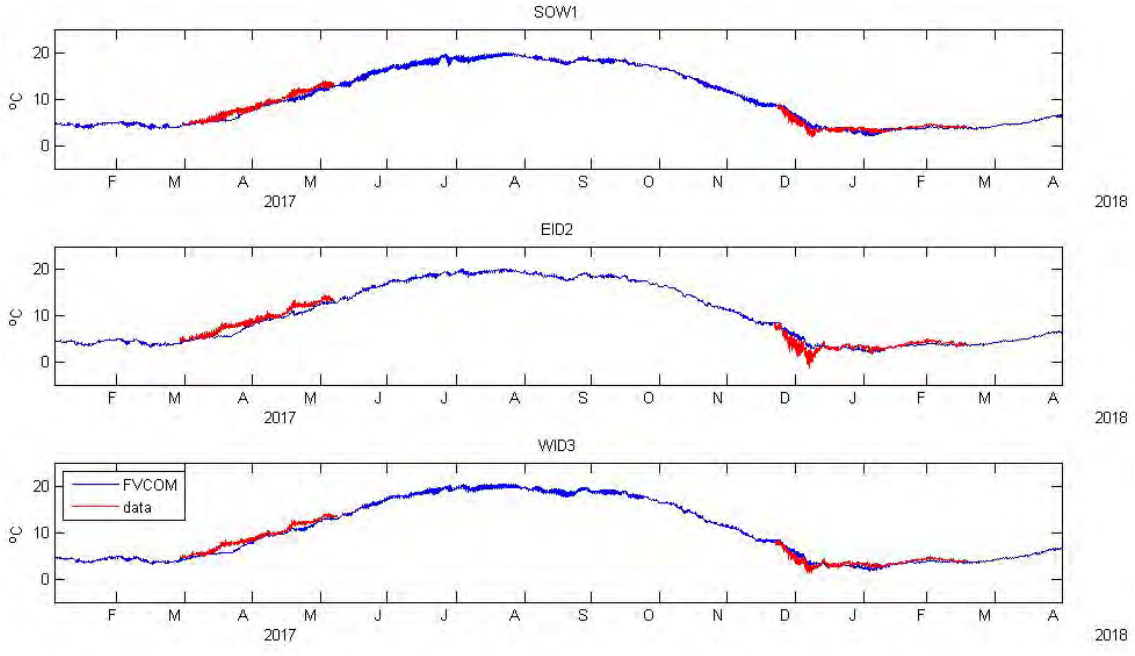

Figure 6.4- 2. Time-series plots of near-bottom temperatures at the three FIS bottom mooring deployment locations comparing the FVCOM predictions (blue) with measurements from the moored instruments.

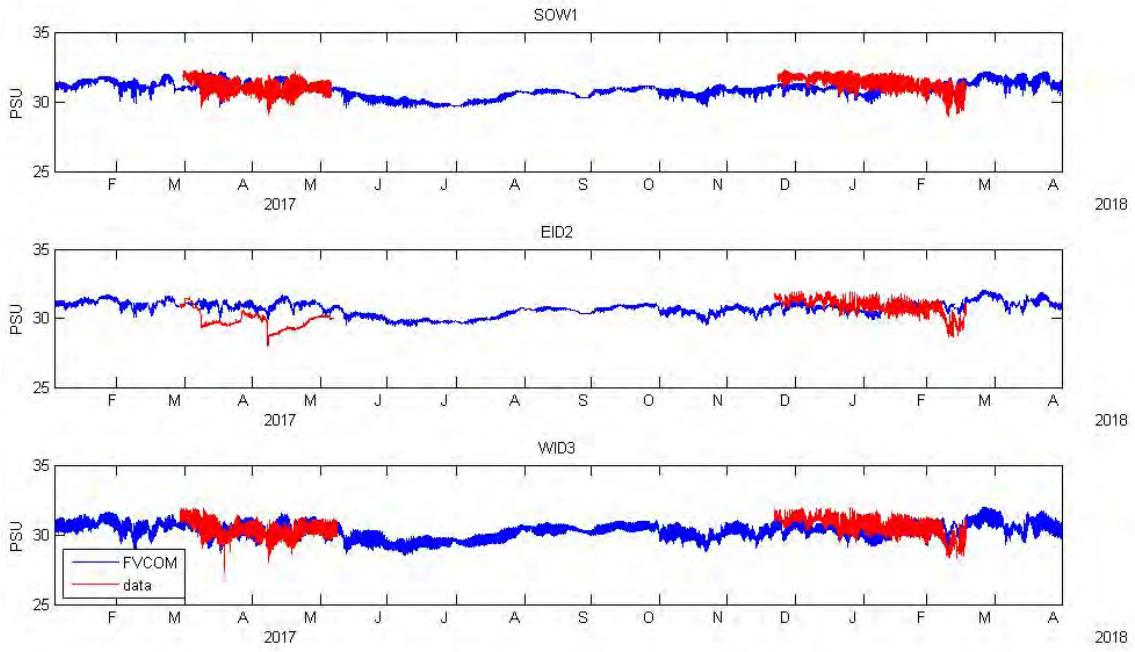

Figure 6.4- 3. Plots of near-bottom salinities at the three FIS bottom mooring deployment locations comparing the FVCOM predictions (blue) with measurements from the moored instruments.

6.5 Acoustic surveys along-track MSL reference heights

The model was used to produce estimates of along-track MSL and water heights to support the acoustic surveys conducted by Roger Flood, Stony Brook University as well as provide further validation of the model results. These surveys took place in Dec 2017, January 2018, and March 2018. Soundings were made at approximately 60k locations and times. Figure 6.5-1 shows the location of these surveys. Figures 6.5-2 and 6.5-3 show the times of the surveys in dark grey at the bottom of the top panel.

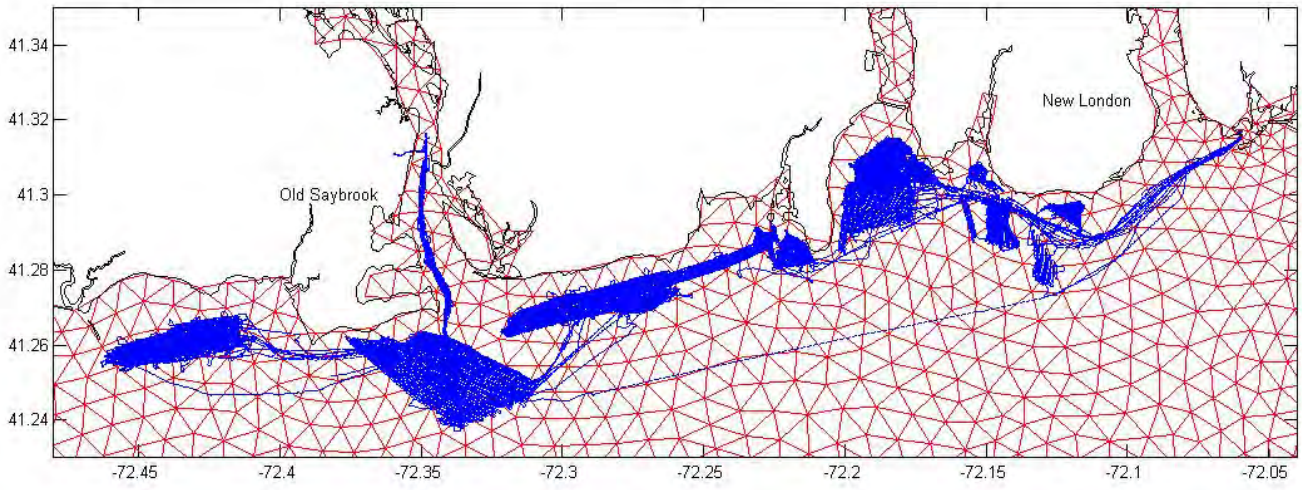

Figure 6.5- 1 Figure 6.5-1. Acoustic survey tracks (blue) for Dec 2017 through Mar 208 surveys, the FVCOM LIS model grid (red), and the CT coastline (black).

In order to remove known errors from the model predictions, the hourly FVCOM LIS SSH solution was compared to the NOAA hourly observations at New London and New Haven and the USGS observations at Old Saybrook. Prior to these comparisons, both the model results and the observations were detided using t_tide (R. Pawlowicz, et al, 2002). The

subtidal and tidal model results were then corrected using the 3-station mean model-observational discrepancy as shown in Eq.2.

$$\eta_{corrected}{}_i^j = \eta_{pred}{}_i^j + \frac{1}{3} \sum_{i=[\,i_{NLN}, i_{HVN}, i_{OS}]} \left(\eta_{obs}{}_i^j - \eta_{pred}{}_i^j \right) \quad (2)$$

where $\eta_{pred}{}_i^j$ are the model SSH predictions at locations $i = [1, \ldots, N]$ and hourly times $j = [1, \ldots, M]$ and $\eta_{obs}{}_i^j$ are the SSH observations at the three gauge locations $i = [i_{NLN}, i_{HVN}, i_{OS}]$ and hourly times $j = [1, \ldots, M]$.

The corrected hourly model results were then temporally interpolated to the 60k unique acoustic survey times using t_tide for the tidal portion and a linear interpolation for the subtidal portion. These time-interpolated results (at the acoustic survey times) were then spatially interpolated from the 200-500 m FVCOM grid to the 60k unique acoustic survey locations. The observations at the three tidal gauges significantly corrects the subtidal model error (which is highly spatially correlated) and, to a lesser extent, the tidal model error, while preserving the spatial gradients in the model. Table 6.5-1 shows the tidal and subtidal skills and RMS errors for both uncorrected and corrected model results.

Also included in table are the skills and errors for a corrected null model. A null model that is corrected by the mean error at the three stations is the mean SSH of the three stations. Because of the high correlation in subtidal SSH in the local region of the three gauges, the corrected null model performs well for subtidal SSHs, particularly at Old Saybrook which is located midway between New London and New Haven. The corrected null model does a poor job with the tides, however.

The results were referenced to NAVD88 by looking at the long-term bias differences between the subtidal model results and the subtidal observations at New London and Old Saybrook, both of which were referenced to NAVD88. Because the model is expected to be able to capture the long-term mean SSH gradients, this also provides a means of comparing the NAVD88 reference for the New London NOAA record with the NAVD88 reference for the USGS Old Saybrook record. There appears to be about a 5 cm difference between these two references. Because the model predicts only a 2 mm difference in the long-term wintertime mean between Old Saybrook and New London, we chose the mean of the NAVS references at these two locations as the “zero” reference and adjusted the model results by a fixed offset accordingly.

Table 6.5- 1. Skills (1-[model-obs]^2⁄var[obs]) and RMS errors (cm) at the three tidal stations for uncorrected model, corrected model, and corrected null model for the period from 1 Dec 2017 through 31 Mar 2018.

			New London	New Haven	Old Saybrook
Tidal	Skill	uncorrected	94.7%	95.2%	90.6%
		corrected	93.6%	99.2%	99.7%
		corrected null	33.0%	81.4%	97.4%
	RMS error (cm)	uncorrected	6.5	14.6	11.0
		corrected	7.2	5.9	2.1
		corrected null	23.3	28.5	5.8
Subtidal	Skill	uncorrected	59.2%	48.0%	57.2%
		corrected	94.0%	93.6%	97.7%
		corrected null	93.9%	95.0%	99.0%
	RMS error (cm)	uncorrected	14.9	18.4	15.5
		corrected	5.7	6.5	3.6
		corrected null	6.1	5.7	2.4
Overall	Skill	uncorrected	80.6%	89.1%	80.5%
		corrected	93.7%	98.5%	99.1%
		corrected null	57.5%	83.0%	98.1%
	RMS error (cm)	uncorrected	16.2	23.4	19.0
		corrected	9.2	8.8	4.0
		corrected null	24.0	29.3	5.9

Figure 6.5-2 shows a comparison of the uncorrected model results with the observations for the period of the March acoustic surveys, while Figure 6.5-3 shows the comparison with the corrected model results. Also shown in the bottom panels of Figs 6.5-2 and 6.5-3 are the model-observation residuals, i.e. the model error. Figure 6.5-2 indicates that this error is highly correlated between the three stations. Since the model is corrected by removing the mean of this error, the remaining error in the corrected model (Fig. 6.5-3) is no longer positively correlated.

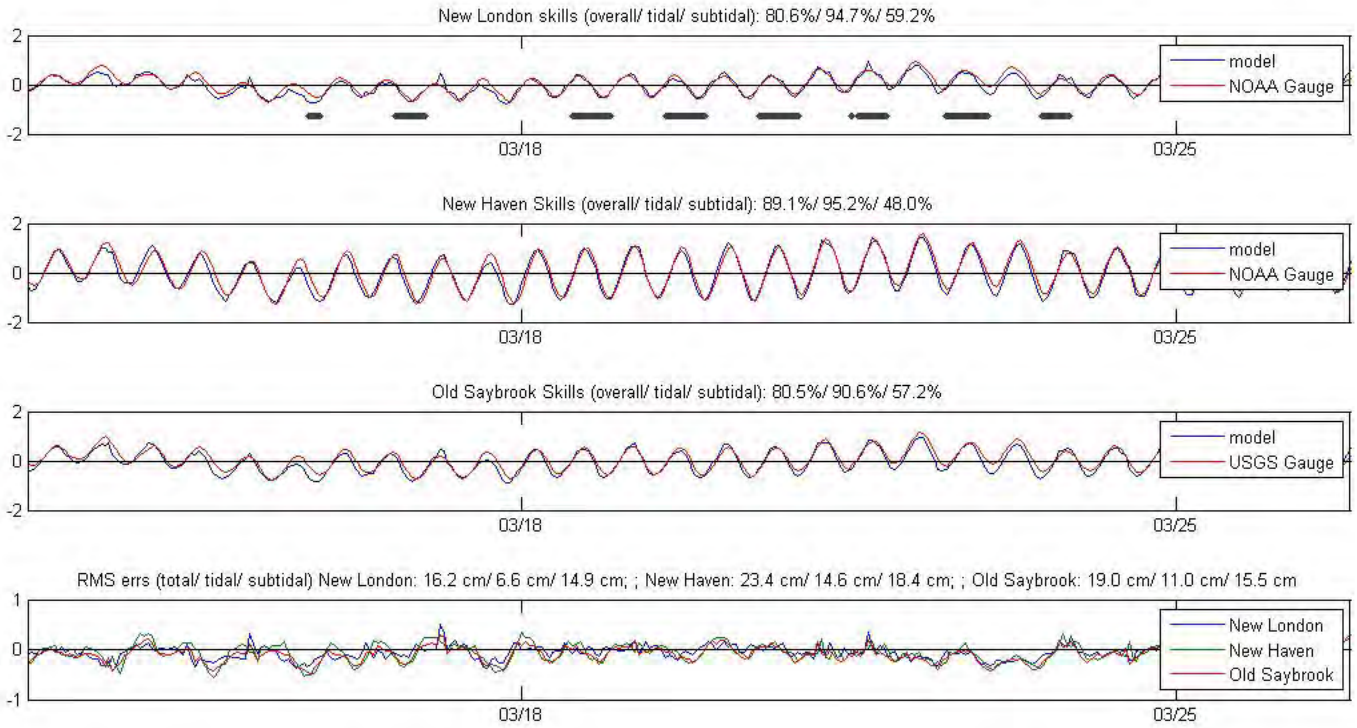

Figure 6.5- 2. Comparison of uncorrected model results (blue) with NOAA gauged observations at New London (top panel) and New Haven (second panel) and with USGS gauged observations at Old Saybrook (3rd panel). The grey dots/ bars in the top panel show the acoustic survey times. The bottom panel shows the differences between the model predictions and the observations for all three stations. Note that these errors are highly correlated.

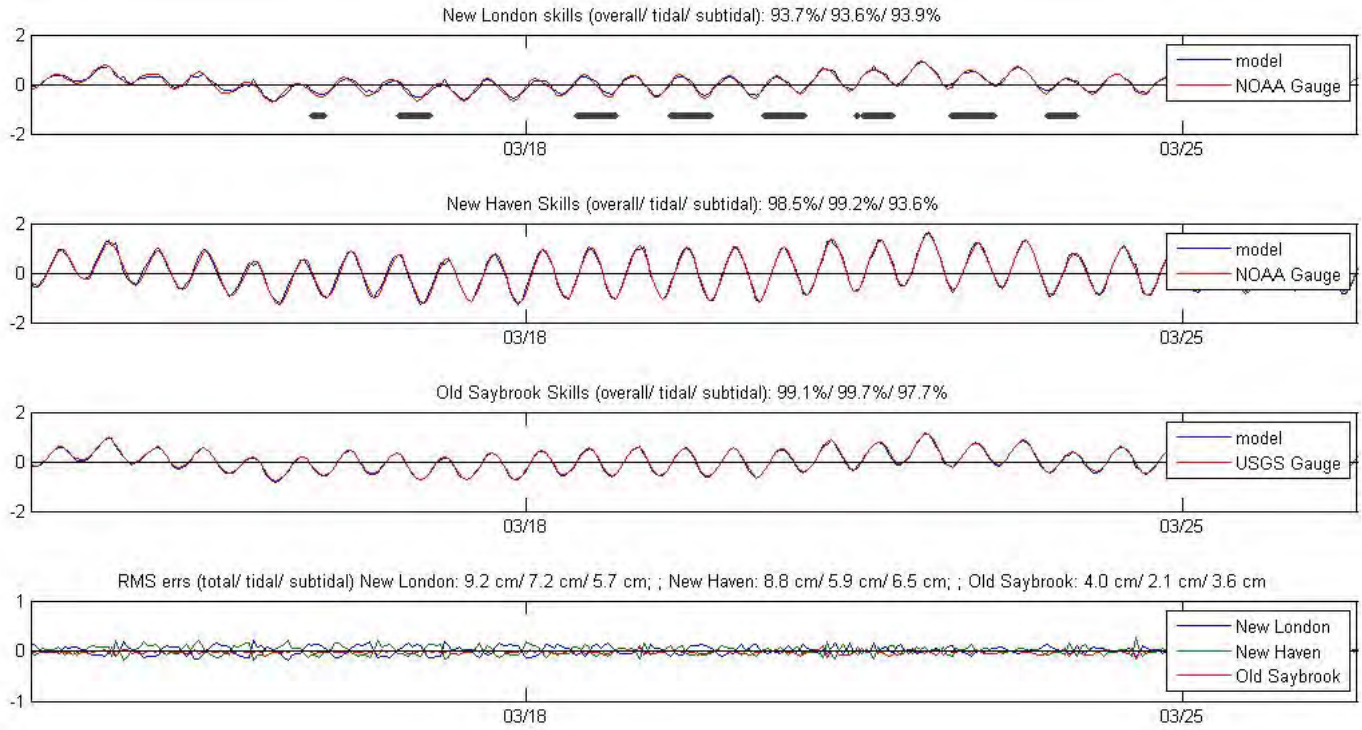

Figure 6.5- 3. Comparison of corrected model results (blue) with NOAA gauged observations at New London (top panel) and New Haven (second panel) and with USGS gauged observations at Old Saybrook (3rd panel). The grey dots/ bars in the top panel show the acoustic survey times. The bottom panel shows the differences between the model predictions and the observations for all three stations. Note that these errors are no longer highly correlated since the correlated error has been removed.

6.6 Physical Oceanographic Products

The model was used to produce maps of:

1. the bottom temperature distributions throughout the study area for each month
2. the bottom salinity distributions throughout the study area for each month
3. the spatial structure of the maximum bottom stress magnitude due to (mainly) tidal currents
4. the spatial structure of the mean bottom stress magnitude due to (mainly) tidal currents
5. tidal and the subtidal currents as (u,v) velocity components where u is the east-west component and v is the north-south component.

These fields were rasterized into GIS format and transferred to the map server to distribute the results. Products are best viewed through that interface. As examples, Figure 6.6-1 shows estimates of mean near-bottom temperatures in the study area during July of 2017, Figure 6.2-2 shows estimates of the maximum bottom stresses due to tidal currents and Figure 6.2-3 depicts the tidal U (east-west) current amplitude. These parameters greatly influence benthic fauna. Note that the magnitude of the spatial gradients predicted by the model far exceeds the estimates of the model error.

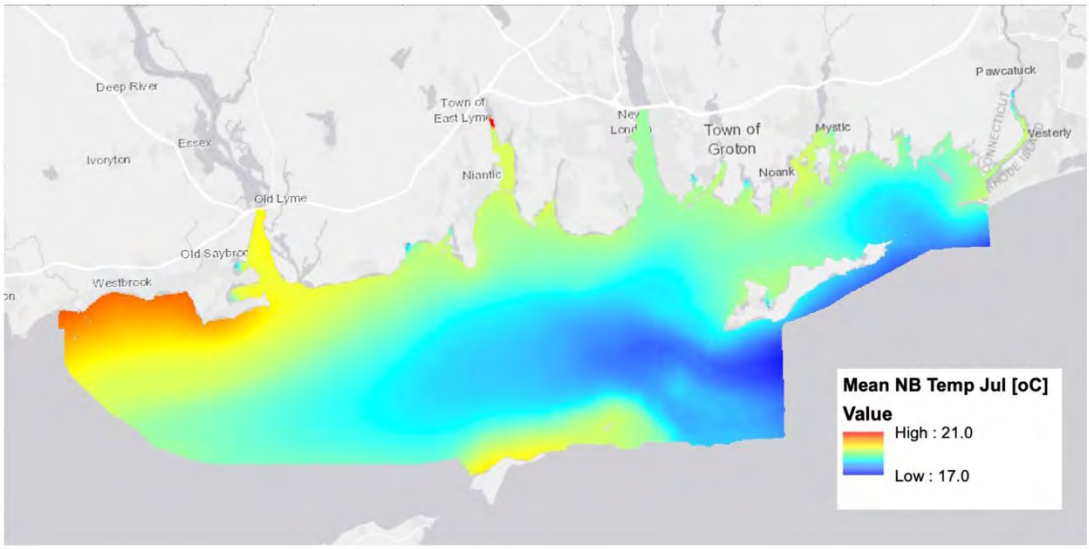

Figure 6.6- 1. Example map product showing mean bottom temperatures during July, 2017.

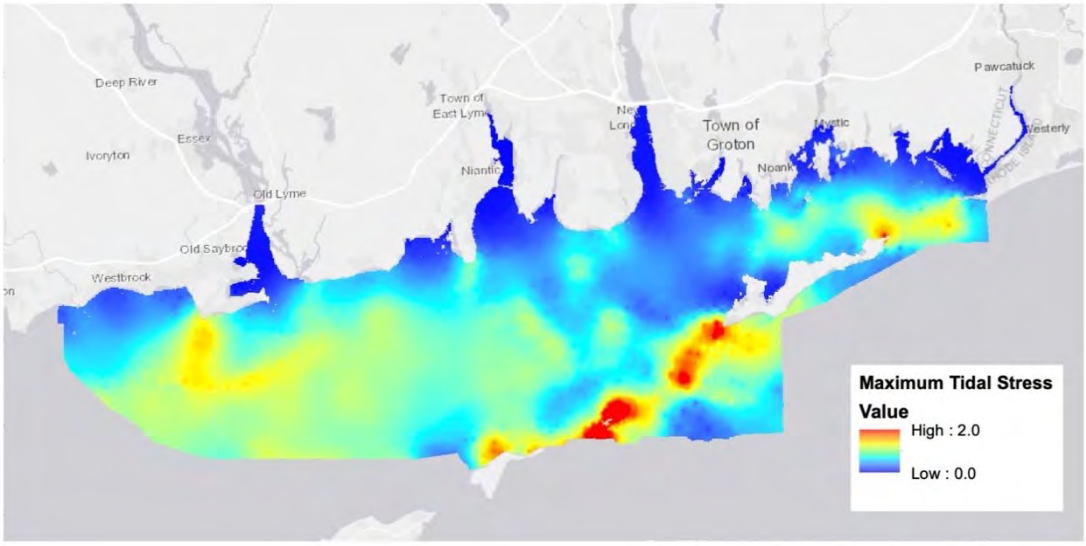

Figure 6.6- 2 Example map product showing maximum bottom stresses due to tides.

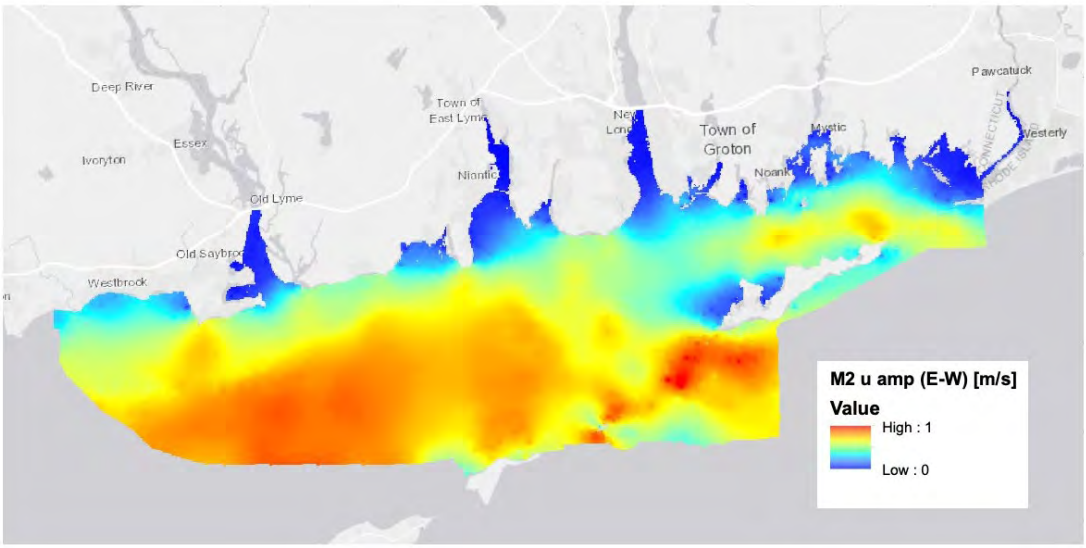

Figure 6.6- 3 Example of map product of mean subtidal currents shown for the u (East-West) component.

6.7 Summary and Conclusions

We report the results of a numerical model to estimate the distributions of ecologically relevant characteristics of the near bottom environment. Using the model, we developed GIS-format map products with information that span the domain. Figure 6.6-1 shows an example. Others are included in the Appendix One.

A limited measurement program was executed to acquire salinity, temperature, and current distributions so that the performance of the model in describing the small-scale spatial variations and the seasonal scale evolution of the variables could be critically assessed. The comparison of the model simulations to observed temperatures is excellent. In the study region, model temperatures were generally well within ±1°C of measured values (See Figure 6.3-2 and 6.4.2). Salinities are generally within ±1 ppt (Figure 6.3-3 and 6.4.3). That the spatial and temporal structures of the temperature, salinity, and velocity fields captured by the model show excellent agreement with the field studies clearly supports the model's use as a tool to interpolate spatially between the observations for the purpose of making maps of the ecologically important characteristics of the bottom environment.

The mean temperature and salinity maps were generated for each month and provide insights into the temporal and spatial variability of these measures within the Phase II area. It is well known that LIS experiences some of the largest seasonal variation in water temperature, which is supported by the model results, with a mean low of 3.5° C occurring particularly in the western regions of the area in the months of February and March. The same western area experiences high water temperature (23°C) in August. Salinity was not surprisingly more stable over the course of the year, with higher salinities occurring in the eastern end of the area and lower salinities near the mouth of the Connecticut during the spring and summer months.

Water currents directly affect benthic organisms through bottom stress, which is a measure of the force the current creates over the seabed. Bottom stress maps were generated for tidal mean, maximum tidal and overall maximum and in each case illustrated similar patterns, with highest values in and around the Race, eastern Fishers Island Sound and to some degree west of the mouth of the Connecticut River. Bottom stress is a key factor in the distribution of sediment types through scouring in high current areas and deposition in lower current regimes. Additionally, bottom stress influences rates of recruitment and feeding by benthic taxa, can impact attachment to the substrates and survivorship during storm events. For these reasons the bottom stress map products were utilized by the Ecological Characterization team as a critical element in the development of the Integrated Habitat Map product.

6.8 References

Bennett, D. C., J. O'Donnell, W.F. Bohlen and A.E. Houk, (2010). Tides and Overtides in Long Island Sound. *Journal of Marine Research*, 68(1), 1-35.

Blumberg, A.F. , L.A. Khan and J. P. St. John, (1999). *Three-Dimensional Hydrodynamic Simulations of the New York Harbor, Long Island Sound and the New York Bight*, Journal of Hydraulic Engineering, 125 799-816.

Bogden, P. S., O'Donnell, J., (1998). Generalized inverse with shipboard current measurements: Tidal and nontidal flows in Long Island Sound. *Journal of Marine Research* 56 (5), 995.

Bokuniewicz, H. J. and R. B. Gordon, (1980a).: Sediment transport and deposition in Long Island Sound. *Advances in Geophysics*, 22, 69-106.

Chen, C.H. Huang, R.C. Beardsley, H. Liu, Q. Xu and G. Cowles, (2007). A finite-volume numerical approach for coastal ocean circulation studies: comparisons with finite difference models. *Journal of Geophysical Research*, 112, C03018, doi:10.1029/2006JC003485.

Crowley, H., (2005). *The seasonal evolution of thermohaline circulation in Long Island Sound*. PhD Dissertation, Marine Sciences Research Center, Stony Brook University, Stony Brook, NY, 142 pp.

Fribance, D. B., J. O'Donnell, *and* A. Houk *(*2013*),* Residual circulation in western Long Island Sound*, Journal of Geophysical Research, Oceans,* 118*,* 4727–4745*, doi:*10.1002/jgrc.20329.

Ganju, N. M. J. Brush, B. Rashleigh, A.L. Aretxabaleta, P. del Barrio, J.S. Grear, L.A. Harris, S.J. Lake, G. McCardell, J. O'Donnell, D.K. Ralston, R.P. Signell, J.M. Testa and J.M.P. Vaudrey. (2016). Progress and Challenges in Coupled Hydrodynamic-Ecological Estuarine Modeling. *Estuaries and Coasts*. 39(2), 311-332.

Hao, Y. , (2008). *Tidal and residual circulation in Long Island Sound*. PhD Dissertation, Marine Sciences Research Center, Stony Brook University, Stony Brook, NY, 70 pp.

Kaputa, N. P. and C. B. Olsen, (2000). State of CT. Dept. of Env. Protection, Long Island Sound Ambient Water Quality Monitoring Program: Summer Hypoxia Monitoring Survey '91-'98 Data Review

Kenefick, A.M., (1985). Barotropic M2 tides and tidal currents in Long Island Sound: a numerical model. *Journal of Coastal Research*, v. 1, 117-128.

Murphy, D.L., (1979). *A Numerical Investigation into the Physical Parameters which Determine the Residual Drift in Long Island Sound*. Ph.D. Dissertation, Dept. of Marine Sciences, The University of Connecticut.

O'Donnell, J. and W.F. Bohlen, (2003). *The structure and variability of the residual circulation in Long Island Sound.* Final Report, Connecticut Department of Environmental Protection, Hartford, CT. Grant CWF 325-R, 303 p. Available at: (http://www.lisrc.uconn.edu/DataCatalog/DocumentImages/pdf/Odonnell_Bohlen_2003.pdf)

O'Donnell, J., R. E. Wilson, K. Lwiza, M. Whitney, W. F. Bohlen, D. Codiga, T. Fake, D. Fribance, M. Bowman, and J. Varekamp (2013). The Physical Oceanography of Long Island Sound. In *Long Island Sound: Prospects for the Urban Sea.* Latimer, J.S., Tedesco, M., Swanson, R.L., Yarish, C., Stacey, P., Garza, C. (Eds.), ISBN-13: 978-1461461258

R. Pawlowicz, B. Beardsley, and S. Lentz, (2002), Classical tidal harmonic analysis including error estimates in MATLAB using T_TIDE, *Computers and Geosciences* (28), 929-937.

Rivera Lemus, E. R., (2008). *Wind waves in central Long Island Sound : a comparison of observations to an analytical expression*. Masters Thesis, Department of Marine Sciences, University of Connecticut.

Schmalz, R.A., Devine, M.F., and Richardson, P.H., (1994). *Residual circulation and thermohaline structure, Long Island Sound Oceanography* Project Summary Report, Volume 2, NOAA Technical Report NOS-OES-003, National Oceanic and Atmospheric Administration, Rockville, MD.

Shchepetkin, A. F. and J. C. McWilliams, (2005). Regional Ocean Model System: a split-explicit ocean model with a free-surface and topography-following vertical coordinate. *Ocean Modelling,* 9, 347–404.

Signell, R., J. List and A. Farris, (2000). Bottom currents and sediment transport in Long Island Sound: a modeling study, *Journal of Coastal Research* 16, 551–566.

Swanson, R.L., (1976). Tides. MESA New York Bight Atlas Monograph, 4. New York Sea Grant Institute. Albany, New York.

Valle-Levinson, A. and R.E. Wilson, (1994a). Effects of Sill Bathymetry, oscillating barotropic forcing and vertical mixing on estuary ocean exchange, *Journal of Geophysical Research,* 99(C6), 12667-12681.

Valle-Levinson, A., and R. E. Wilson, (1994b). Effects of sill processes and tidal forcing on exchange in eastern Long Island Sound, *Journal of Geophysical Research*, 99(C6), 12667-12681Valle-Levinson et al. (1995)

Wilson, R.E. and R.L. Swanson. (2005). A perspective on bottom water temperature anomalies in Long Island Sound during the 1999 Lobster Mortality event. *Journal of Shellfish Research,* 24, 825–830.